Nanoscale

ROYAL SOCIETY OF CHEMISTRY

PAPER

View Article Online
View Journal | View Issue

Check for updates

Cite this: *Nanoscale*, 2023, **15**, 8424

Design of Raman reporter-embedded magnetic/plasmonic hybrid nanostirrers for reliable microfluidic SERS biosensors†

Bingfang Zou,[a,b] Shiyun Lou, [a] Jie Duan,[a] Shaomin Zhou*[a] and Yongqiang Wang *[a]

Received 19th January 2023,
Accepted 28th March 2023

DOI: 10.1039/d3nr00303e

rsc.li/nanoscale

Magnetic-based microfluidic SERS biosensors hold great potential in various biological analyses due to their integrated advantages including easy manipulation, miniaturization and ultrasensitivity. However, it remains challenging to collect reliable SERS nanoprobe signals for quantitative analysis due to the irregular aggregation of magnetic carriers in a microfluidic chamber. Here, magnetic/plasmonic hybrid nanostirrers embedded with a Raman reporter are developed as capture carriers to improve the reliability of microfluidic SERS biosensors. Experimental results revealed that SERS signals from magnetic hybrid nanostirrers could serve as microenvironment beacons of their irregular aggregation, and a signal filtering method was proposed through exploring the relationship between the intensity range of beacons and the signal reproducibility of SERS nanoprobes using interleukin 6 as a model target analyte. Using the signal filtering method, reliable SERS nanoprobe signals with high reproducibility could be picked out from similar microenvironments according to their beacon intensity, and then the influence of irregular aggregation of magnetic carriers on the SERS nanoprobe could be eliminated. The filtered SERS nanoprobe signals also exhibited excellent repeatability from independent tests, which lay a solid foundation for a reliable working curve and subsequent accurate bioassay. This study provides a simple but promising route for reliable microfluidic SERS biosensors, which will further promote their practical application in biological analysis.

Introduction

Microfluidic devices have been gaining increasing attention in the field of chemical sensing and biosensing because of their advantageous features, including flexible scale-up, precise control of fluids, low sample and reagent consumption, and rapid sample processing.[1–3] In particular when nanomaterials were integrated into microfluidic devices, the detection sensitivity and efficiency were improved greatly.[4–6] For example, fluorescent nanomaterials like highly bright QDs have been used as optical nanoprobes in microfluidic devices, which exhibited much higher signals than traditional fluorophores in protein diagnostics.[7,8] Recently, surface-enhanced Raman spectroscopy (SERS), which provides ultrahigh sensitivity and a narrow spectral width with higher multiplexing capabilities, has been emerging as a superior analysis technique.[9–11] The combination of microfluidics and SERS nanoprobes opens up a new technical platform, which has aroused great interest from researchers in various fields.[12–14] Nowadays, a wide range of state-of-the-art plasmonic nanomaterials have been designed as active substrates of ultrasensitive and encoded SERS nanoprobes, which led to the vigorous development of microfluidic SERS biosensors.[15]

In microfluidic SERS sensors, great efforts have also been made on the design of capture carriers for convenient, low-cost and highly efficient microfluidic biosensors.[16–18] Compared with planar substrates, magnetic particles are much more attractive as capture carriers due to their high surface-to-volume ratio and magnetic responsiveness, which could reduce the assay time during target binding and detection steps greatly.[19–23] Additionally, special magnetic manipulations also help simplify and miniaturize the device.[24] For example, Chen *et al.* developed a simple microfluidic system using magnetic particles as capture carriers, where the assay time was reduced from 4 hours to 80 minutes due to magnetic responsiveness, and the detection specificity was also enhanced.[25] Recently, magnetic particles were assembled into

---

[a] *Key Lab for Special Functional Materials of Ministry of Education, School of Materials Science and Engineering, Henan University, Kaifeng 475004, China. E-mail: wangyq@henu.edu.cn, smzhou@henu.edu.cn*

[b] *School of Physics and Electronics, Henan University, Kaifeng 475004, P. R. China*

† Electronic supplementary information (ESI) available: Supplementary experimental section, figures and movies. See DOI: https://doi.org/10.1039/d3nr00303e

a chain-like structure and employed as capture carriers in microfluidic SERS biosensors by Xiong *et al.*[26] Since they acted as nanostirrers under automatic magnetic manipulation, high mixing efficiency and reproducible aggregation could be achieved in the microfluidic platform.[27–30] At present, magnetic-based microfluidic SERS biosensors have demonstrated great potential in trace and multiplex biological analysis of disease-related proteins, microRNAs, cytokines and so on.[31–33]

However, when magnetic particles were used as carriers in biosensors, irregular aggregates containing magnetic carriers, analytes and SERS nanoprobes were generated finally under an external magnet. The resultant varying microenvironment made it rather complex to collect reliable SERS nanoprobe signals for quantitative sensing, which is different from the case of a uniform planar substrate.[34,35] Although magnetic particle carriers could be concentrated densely in a microfluidic chamber under automatic electromagnetic manipulation, the above problems are still unavoidable. As a matter of fact, it has always been a vital but challenging issue to collect reliable SERS nanoprobe signals for biosensors, which varied greatly with sampling parameters, substrate uniformity and other factors.[36–39] Recently, SERS mapping of the bead carrier was put forward to obtain reliable SERS nanoprobe signals through averaging all signals, where varying microenvironments were encountered due to their spherical surface, but it was too time-consuming and costly.[40] Therefore, it remains challenging to acquire reliable signals efficiently for magnetic-based microfluidic SERS biosensors.

In view of the differences between sampling microenvironments, we propose that reliable SERS nanoprobe signals could be collected from those microenvironments with negligible differences. The designed strategy was illustrated in Scheme 1, wherein (a) magnetic/plasmonic hybrid nanostirrers embedded with a Raman reporter were developed as carriers. Meanwhile, ultrasensitive SERS nanoprobes with spiky Au cores were synthesized to label analytes. (b) After they were injected into the microfluidic platform at the same time, the sandwich complex formed through an immune reaction was accumulated into dense aggregates in a chamber under magnetic manipulation. (c) Under such conditions, both SERS signals from irregular aggregates of magnetic carriers and SERS nanoprobes could be collected simultaneously under Laser irradiation. Using interleukin 6 as a model target analyte, experimental results exhibited that the SERS signals from irregular aggregates of magnetic carriers could serve as microenvironment beacons. A signal filtering method was proposed by systematically exploring the relationship between the intensity range of beacons and the signal reproducibility of SERS nanoprobes, where similar sampling microenvironments could be determined according to the beacon intensity. The filtered signals exhibited high reproducibility and repeatability using the established signal filtering method, and it was further demonstrated that quantitative bioassays with overall accuracies over 92% could be achieved by the designed magnetic-based microfluidic SERS biosensor.

Experimental section

Materials

Ferric chloride hexahydrate ($FeCl_3 \cdot 6H_2O$), poly(acrylic acid) (PAA, 2000), sodium acetate (NaAc), ethylene glycol, polyvinyl pyrrolidone (PVP, 4K), L-ascorbic acid (AA), potassium iodide (KI), hydrogen tetrachloroaurate (III) trihydrate ($HAuCl_4 \cdot 3H_2O$), pyrrole, hydrochloric acid (HCl, 37%), ammonia ($NH3 \cdot H_2O$), tetraethyl orthosilicate (TEOS), 4-mercaptobenzoic acid (MBA), and 2,3,5,6-tetrafluorothiophenol (TFTP) were purchased from Aladdin Reagent Company (China). PDMS (Sylgard 184 Silicone Elastomer Kit) was purchased from Dow Corning (MI, U.S.A.). Interleukin 6 (IL-6) and its antibodies, procalcitonin (PCT) and C-reactive protein (CRP) were purchased from Shanghai Linc-Bio Science Co. (China).

Synthesis of Fe_3O_4/Au hybrid nanostirrers

Fe_3O_4 nanospheres (~400 nm) were synthesized by a modified solvothermal method according to our previous report.[41] After being modified with APTES, Au nanoparticles (5 nm) were absorbed onto Fe_3O_4 nanospheres as seeds. Rough Au shells on Fe_3O_4 nanospheres were achieved through interfacial seed-mediated growth. In detail, Fe_3O_4 nanospheres with Au seeds (40 mg) were firstly dispersed in 100 ml of PVP-AA-KI solution using a mechanical stirrer, including PVP (0.2 wt%), L-ascorbic acid (1.2 mM) and KI (4.5 mM). After 1 ml of $HAuCl_4$ (25 mM) was injected into the above solution, Fe_3O_4/Au hybrid nanospheres were synthesized after 0.5 h, and separated using an external magnet and washed with deionized water repeatedly.

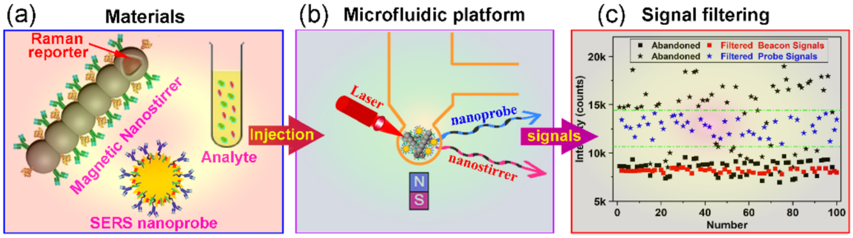

Scheme 1 The illustration of reliable microfluidic SERS biosensor by using Raman reporter-embedded magnetic/plasmonic hybrid nanostirrers as capture carriers. (a) Raman reporter-embedded magnetic/plasmonic nanostirrer, analyte, and SERS nanoprobe. (b) Raman signal acquisition of the sample concentrated in small chamber of the microfluidic platform. (c) Filter out reliable SERS nanoprobe signals based on beacons' intensity.

The Fe_3O_4/Au hybrid nanospheres were dispersed in the MBA/PVP mixture and a thin silica layer was coated through the Stöber method.

The silica coated Fe_3O_4/Au-MBA hybrid nanospheres were used as building blocks of nanochains. During the magnetic assembly, a neodymium iron boron magnet with a disk shape (10 cm in diameter, 950 G) was used to provide a gradient magnetic field. A solution containing the above synthesized building blocks (12 mL), ammonia (2 mL) and TEOS (0.2 mL) was placed on the top of the disk magnet at a distance of about 4 cm. After the solution was exposed to the magnet field for a determined time, it was transferred into a rotary mixer and reacted for 1 hour. After repeated washing, Fe_3O_4/Au hybrid nanostirrers could be obtained. The average length of Fe_3O_4/Au hybrid nanostirrers could be adjusted by the time exposed to the magnetic field.

Fabrication of the PDMS microfluidic platform

The PDMS microfluidic device was fabricated by standard soft lithography and rapid prototyping methods. A positive SU-8 100 photoresist mould was fabricated on a silicon wafer using a transparent mask. The PDMS prepolymer and curing agent (Sylgard 184, Dow Corning) were mixed in a 10 : 1 ratio (w/w), degassed under vacuum, and then decanted onto the fabricated SU-8 mould. A neodymium magnet was placed in position, and the mixture was cured at 70 °C for 2 h in an oven. After curing, the PDMS replica was peeled from the master mould. Two inlet holes and one outlet hole were punched for fluidic access, and the PDMS replica was aligned to a glass slide in oxygen plasma to achieve firm adhesion. The main channel was 100 μm in width. The big mixing chamber and small concentrating chamber were 1000 and 100 μm in diameter, respectively. The depth of all channels and chambers was 50 μm.

Detection of IL-6 using the designed microfluidic SERS sensor

The magnetic hybrid nanostirrers and SERS nanoprobes were conjugated with antibodies before use, and antibody conjugating procedures are described in the ESI.† For the detection of IL-6, 1 μL of analyte solution and 1 μL of a solution containing magnetic hybrid nanostirrers and SERS nanoprobes were injected into the microfluidic platform. The two solutions were then mixed within a big chamber. The magnetic hybrid nanostirrers and SERS nanoprobes that were decorated with IL-6 antibodies were incubated with IL-6 in the above microfluidic platform for 10 minutes at 37 °C under a rotating magnetic field. After SERS nanoprobes conjugated magnetic nanostirrers were concentrated in a small chamber, SERS measurements were performed using a Renishaw confocal Raman microscope equipped with 785 nm lasers. The laser beam with a power of 0.5 mW was focused with a 20× objective. A single-point measurement with an integration time of 20 s was performed for each spectrum acquisition. In order to achieve a working curve, a series of IL-6 concentrations ranging from 10 fg mL^{-1} up to 10 μg mL^{-1} were performed using the above procedure.

Characterization

Scanning electron microscopy (SEM) images were taken with a JEOL JSM-7001F microscope operating at 5 kV. Transmission electron microscopy (TEM) images and high-resolution TEM (HRTEM) images were recorded on a Hitachi H-7650 microscope at an accelerating voltage of 200 kV, respectively. The compositions were investigated by X-ray powder diffraction (RIGAK, D/MAX 2550 VB/PC). Zeta potential measurements were performed with a Nano Zetasizer (Malvern). The magnetic properties of the products were characterized with a superconducting quantum interference device magnetometer (SQUID, MPMSXL-7) at 300 K. A PSM-1000 microscope (Motic, Germany) equipped with a camera was used to record the rotation of magnetic nanostirrers, where the rotating magnetic field was set up by mounting four electromagnetic coils on a cross-shaped plastic plate.

Results and discussion

In our experiment, magnetic/plasmonic hybrid nanostirrers embedded with a Raman reporter were synthesized according to the designed procedure in Fig. 1a. A thin Au shell was first deposited on Fe_3O_4 nanospheres as an active SERS substrate of the Raman reporter. And then the Fe_3O_4/Au hybrid nanospheres were coated with a thin silica layer as building blocks, they were guided into a chain-like structure and further solidified into an Fe_3O_4/Au hybrid nanostirrer by silica coating. During the magnetic assembly, the interparticle dipole–dipole potential in a gradient magnetic field was utilized to overcome thermal fluctuations.[42] Here, superparamagnetic Fe_3O_4 nanospheres with a diameter of about 400 nm were synthesized as magnetic cores in our experiments as shown in Fig. 1b. The rough Au shell was deposited on Fe_3O_4 nanospheres through seed-mediated heterogeneous growth in Fig. 1c, and the thiol Raman reporter MBA was adsorbed rigidly on a Au shell through Au–S bond interactions. During the magnetic guided self-assembly, when the MBA-modified Fe_3O_4/Au nanospheres were directly used as building blocks of nanochains firstly, only a coarse silica coating was observed on the surface of Fe_3O_4/Au hybrid nanochains as seen in Fig. 1d, which could be attributed to the incompatibility between Au and silica layers. Meanwhile, some of the nanochains even aggregated together due to the lack of repulsive forces between them. Thus, a thin silica layer was necessary to be precoated on the MBA-modified Fe_3O_4/Au hybrid nanospheres for improved dispersibility and silica deposition during the assembly process. When silica coated Fe_3O_4/Au nanospheres were used as building blocks (Fig. 1e and f), dispersible Fe_3O_4/Au hybrid nanostirrers with smooth silica shells were achieved as shown in Fig. 1g. The extinction spectra including Fe_3O_4/Au hybrid nanospheres and Fe_3O_4/Au hybrid nanostirrers were characterized as seen in Fig. S1,† where the red shift of the plasmon resonance peak from 915 to 1045 nm was clearly observed. Meanwhile, the red shift of the peak, which was caused by interparticle coupling, proved the formation of Fe_3O_4/Au

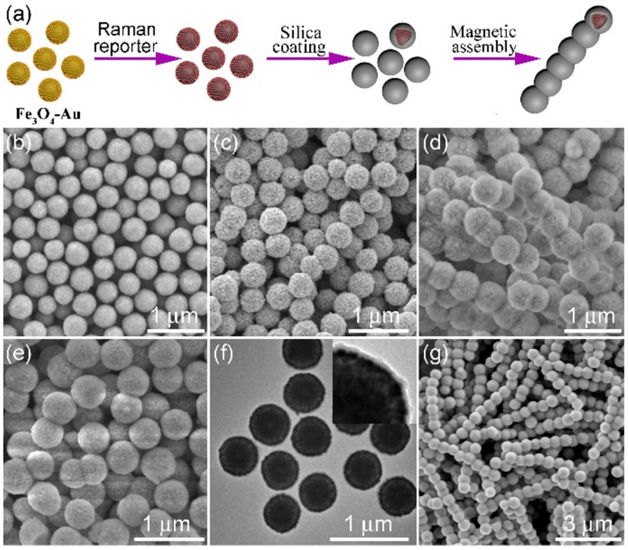

Fig. 1 (a) Schematic processes of synthesizing magnetic Au hybrid nanostirrers. SEM images of (b) Fe_3O_4 nanospheres, (c) MBA-modified Fe_3O_4/Au hybrid nanospheres and (d) Fe_3O_4/Au hybrid nanostirrers using product (c) as building blocks. (e) SEM image and (f) TEM image of MBA-modified Fe_3O_4/Au hybrid nanospheres with a thin silica coating. (g) SEM image of Fe_3O_4/Au hybrid nanostirrers using product (e) as building blocks.

hybrid nanostirrers indirectly. During the synthesis of magnetic hybrid nanostirrers, Fe_3O_4 nanospheres with different sizes were also investigated. For example, smaller size Fe_3O_4 nanospheres (280 nm) were used as the core to synthesize Fe_3O_4/Au nanospheres as building blocks, but only several dimers or trimers were synthesized using similar conditions as seen in Fig. S2.† As a matter of fact, pure Fe_3O_4 nanospheres even with a small size could be assembled into nanochains, which has been reported previously.[43] Here, the failure to synthesize Fe_3O_4/Au hybrid nanostirrers should be attributed to the Au shell, which decreases the magnetic moment of the building block greatly, since the density of Au (19.32 g cm^{-3}) is about 4 times that of Fe_3O_4 (5.18 g cm^{-3}). Thus, the interparticle attraction force between Fe_3O_4/Au hybrid nanospheres becomes too weak when compared with Brownian motion, and cannot bind the adjacent Fe_3O_4/Au hybrid nanospheres together under the same conditions. When big Fe_3O_4 nanospheres (600 nm) were used as cores, the saturated magnetic moment of hybrid nanospheres increased, but only separated particles were observed (Fig. S3†). We speculate that big Fe_3O_4 nanospheres have large inertia of motion during the mixing process, which can break the free silica bridge between building blocks formed in the early stage. When using 500 nm Fe_3O_4 nanospheres, nanochains can be obtained, but the length is not uniform (Fig. S4†). Therefore, both surface and magnetic properties should be considered after introducing the Au shell, and Fe_3O_4 nanospheres with diameters around 400 nm are suitable magnetic cores from the above control experiments.

The as-synthesized Fe_3O_4/Au hybrid nanostirrers were characterized systematically in Fig. 2. The difference between XRD patterns (I) and (II) demonstrated the main compositions in Fe_3O_4/Au hybrid nanostirrers, which could be identified from their characteristic diffraction peaks, marked by rectangles (Fe_3O_4), circles (Au), and triangles (silica), respectively. To determine their distribution, elemental mapping images including Fe, Au, Si, and S are presented in Fig. 2b, where the inner Fe_3O_4 core, the intermediate Au layer and the outer silica shell corresponded to the distribution graphs of Fe, Au and Si, respectively. Besides, the S element could be distinguished clearly as well, which was from the Raman reporter MBA. And the strong characteristic Raman peak of MBA at 1075 cm^{-1} could be observed in the Raman spectrum in Fig. 2c, which resulted from the SERS enhancement of the rough Au shell. The magnetic properties of the as-obtained nanostirrers that were inherited from Fe_3O_4 cores were characterized as shown in Fig. 2d, where the magnetic hysteresis with nearly zero coercivity revealed its superparamagnetism, and the saturated

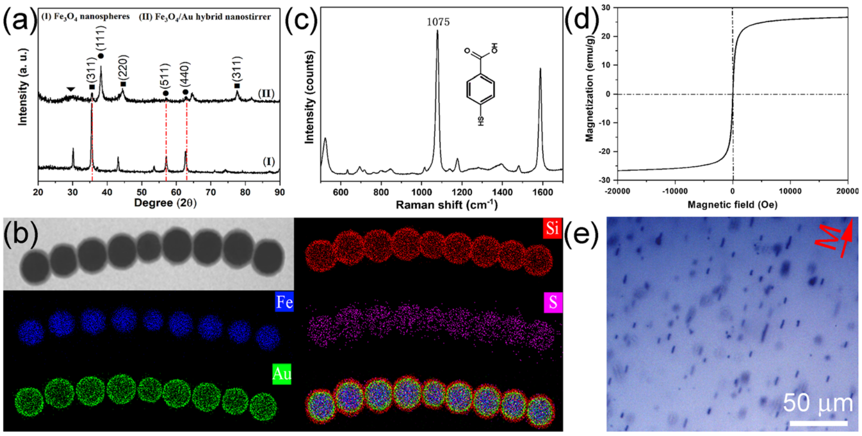

Fig. 2 (a) XRD patterns of Fe_3O_4 nanospheres and Fe_3O_4/Au hybrid nanostirrers. (b) Elemental mapping of a single Fe_3O_4/Au hybrid nanostirrer. (c) SERS spectrum of MBA embedded-Fe_3O_4/Au hybrid nanostirrers. (d) Magnetic hysteresis of Fe_3O_4/Au hybrid nanostirrers. (e) Optical images of Fe_3O_4/Au hybrid nanostirrers aligned under a rotating magnetic field.

magnetic moment was about 26 emu g^{-1}. Optical characterization (Fig. 2e) showed the as-synthesized magnetic hybrid nanostirrers aligned immediately in a magnetic field, which took synchronous and localized rotation when two pairs of orthogonal electromagnetic coils were activated periodically (ESI Movie S1†). When they were used as capture carriers in a microfluidic platform, they can rotate in a big chamber to capture the analytes, and then aggregate in a small chamber under magnetic manipulation (Fig. S5, ESI Movie 2†).

Interleukin-6 (IL-6), a kind of glycoprotein, is widely involved in the production of inflammation as a proinflammatory factor. In particular in acute inflammation, elevated IL-6 levels are often used to determine the inflammatory response triggered by bacterial infection.[44,45] Thus, it is urgently required to develop a more advanced, reliable and rapid technique to detect IL-6 in complex biological systems. Here in our experiment, IL-6 was used as a model target analyte. Raman reporter embedded magnetic hybrid nanostirrers were modified with capture antibodies of IL-6 as carriers. In addition, spiky Au nanoparticles were synthesized as the plasmonic core of SERS nanotags, which could enhance the Raman reporter TFTP greatly.[46] And then highly brilliant SERS nanoprobes were fabricated by conjugating capture antibodies of IL-6 on the above SERS nanotags (Fig. S6 and S7†). Using magnetic hybrid nanostirrers as carriers, we demonstrate that IL-6 could be detected rapidly and reliably on microfluidic SERS sensors according to our designed strategy.

When magnetic hybrid nanostirrers are used as capture carriers of microfluidic devices, their length has a great influence on the detection of target analytes.[24] Here in our experiment, magnetic hybrid nanostirrers with different lengths were firstly synthesized by tailoring the exposure time to the magnetic field as shown in Fig. 3a. When exposure times were set at 10 s, 20 s, 40 s and 60 s, the average lengths of the magnetic hybrid nanostirrers were 1 μm, 3 μm, 5 μm, and 12 μm, respectively. Longer magnetic nanostirrers could reach 20 μm by extending the exposure time to 120 s, but most of them stuck together side by side (Fig. S8†), which makes them unsuitable as capture carriers due to their nonuniformity. By using the above magnetic hybrid nanostirrers (I–IV) as carriers, the effect of their length on the capture rate was then investigated by using IL-6 (1 ng mL^{-1}). As shown in Fig. 3b, the vertical coordinate represents the capture percentage, which was defined as the ratio of average signal intensities at the sampling time to that at the saturated adsorption time. It could be found that the capture percentage increased with sampling intervals for all magnetic hybrid nanostirrers. In detail, it took nanostirrers III and IV about 8 and 6 minutes to reach saturated adsorption, while longer times were needed for shorter nanostirrer II (30 minutes) and nanostirrer I (45 minutes), respectively. Apparently, longer nanostirrers perturbed more solution at the same rotating speed, which makes more analytes diffuse to the surface of nanostirrers.

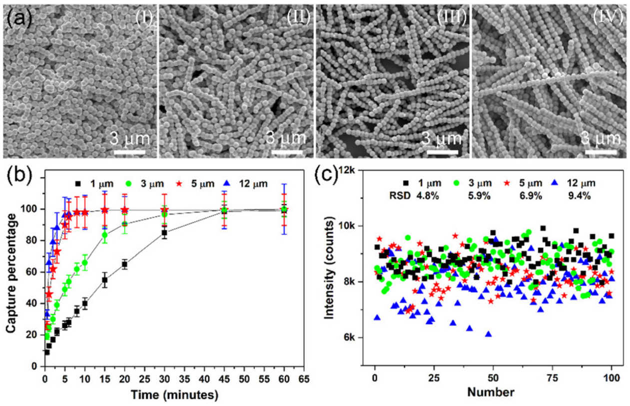

Fig. 3 (a) SEM images of magnetic hybrid nanostirrers (I–IV) synthesized by regulating the exposure time to the magnetic field. (b) Capture rates of magnetic hybrid nanostirrers (I–IV) and (c) SERS signals of magnetic hybrid nanostirrers (I-IV) aggregated in a small chamber.

Meanwhile, when magnetic hybrid nanostirrers were gathered in a microfluidic chamber under an external magnetic field, it can be imagined that aggregates with different stacking would form due to their differences in length. The disorder degrees were studied by recording one hundred SERS signals from four kinds of aggregates, respectively. As shown in Fig. 3c, the signals collected from all aggregates fluctuated greatly in intensity, and the fluctuating range became wider with their lengths. The relative standard deviation (RSD) values of the signals, which could reflect the difference of sampling points, were calculated to be 4.8% (1 μm), 5.9% (3 μm), 6.9% (5 μm) and 9.4% (12 μm), respectively. The increased RSD values implied that the longer the magnetic hybrid nanostirrers are, the more disorder they stacked in a small chamber. For example, the RSD value of nanostirrer IV reached 9.4%, much higher than that of nanostirrer I (4.9%). Considering that the aggregation state of the magnetic hybrid carriers affected the distribution of SERS nanoprobes greatly, shorter nanostirrers are better carriers from the viewpoint of probe signals.

From the above results, the capture rate and disorder degree are two irreconcilable factors when magnetic hybrid nanostirrers with different lengths are used as capture carriers. In the case of fast capture of target analytes, the nanostirrer III (5 μm) with a lower disorder degree of aggregates is the optimal capture carrier in the present experiment. Even though the optimal magnetic hybrid nanostirrers (5 μm) were used as carriers, it is still necessary to consider the influence of their irregular aggregation on the distribution of SERS nanoprobes in order to achieve reliable detection.

According to our designed strategy, the influence of irregular aggregates of magnetic hybrid nanostirrers on the distribution of SERS nanoprobes could be eliminated by picking out similar sampling microenvironments. Here, the relationship between the SERS signals from irregular aggregates of magnetic carriers and SERS nanoprobe signals was investigated for the first time. As shown in Fig. 4a, one hundred Raman spectra were first collected randomly by single-point acquisition. The Raman peaks at 1075 cm^{-1} and 1370 cm^{-1} could be assigned to the Raman reporter MBA in magnetic

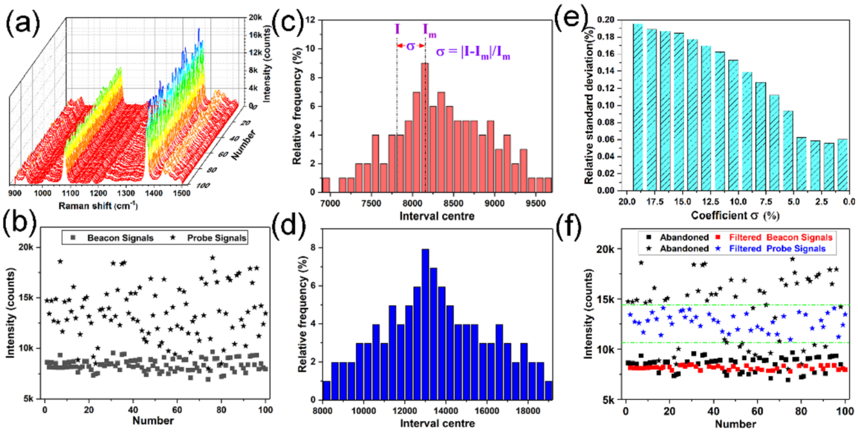

Fig. 4 (a) Raman spectra collected through random single-point measurements from one hundred points. (b) The intensity distributions of the beacon signal (1075 cm^{-1}) and probe signal (1370 cm^{-1}). Column chart of the (c) beacon signal with an intensity interval of 100 counts and the (d) probe signal with an intensity interval of 400 counts. (e) Relative standard deviation of the filtered probe's signals with different *s* values. (f) Filtering SERS nanoprobe signals according to the beacon intensity (σ = 4.3%).

hybrid nanostirrers and TFTP in SERS nanoprobes, respectively. After the two SERS signals were collected and plotted into two kinds of intensity distribution marked with squares and asterisks in Fig. 4b, it can be found that both the signals have similar variation tendencies on the whole. When the two signals were plotted into a column chart with intensity intervals of 100 counts and 400 counts respectively, both of them exhibited a skewed distribution as shown in Fig. 4c and d. As we know that on a planar carrier, the random immunoconjugated SERS nanoprobes lead to the normal distribution of signals, and here the skewed distribution of SERS nanoprobe signals revealed the great influence of irregular aggregation of magnetic carriers.[35] It is noted that although different aggregation states of magnetic carriers may produce similar SERS signals, their skewed distribution implied that these SERS signals could represent their aggregation state to some degree. In other words, the SERS signals from irregular aggregates of magnetic carriers could serve as sampling microenvironment beacons during the measurement. Additionally, when repeated independent tests were performed, similar skewed distributions of the two signals were also obtained as shown in Fig. S9,† which indicated that a reproducible aggregation state could be achieved on a microfluidic platform with automatic electromagnet manipulation.

Using SERS signals from irregular aggregates of magnetic carriers as microenvironment beacons, SERS nanoprobe signals in a similar microenvironment could be picked out according to the beacon intensity. Here, a signal filtering method was developed by exploring the relationship between the intensity range of beacons and the signal reproducibility of SERS nanoprobes. Firstly, the sampling microenvironments with maximal frequency (I_m) was picked out from the distribution diagram of the beacon in Fig. 4c, the corresponding beacon intensity is centred at about 8150 counts. The beacon intensity deviation coefficient (σ), which was defined by $|I - I_\text{m}|/I_\text{m}$, reflected the similarity of sampling microenvironments, where the smaller the σ value, the higher the similarity of the sampling microenvironment. As seen in Fig. 4e, when we narrowed the intensity deviation gradually, it was found that the RSD values of the filtered SERS nanoprobe signals became small as σ decreased. In detail, the RSD value of original SERS nanoprobe signals was as high as 19.6%, but the RSD value of the filtered signals decreased to 6.0% when σ reached 4.3%, and then the RSD values fluctuated a little between 5.6% and 6.2%. The similar downward trend of RSD and σ indicated that the aggregated state of magnetic hybrid nanostirrers indeed affected the distribution of SERS nanoprobes greatly. Meanwhile, the little change of RSD with σ ranging from 4.3% to 0.6% revealed that the influence of the microenvironment on SERS nanoprobe signals was no longer a major factor in such intervals. And the random attachment of SERS nanoprobes on magnetic hybrid nanostirrers was speculated to be dominant. It is worth noting that the amount of filtered data decreases rapidly as σ became smaller, which will then increase the difficulty in filtering reliable data. Therefore, the σ value at 4.3% was considered to be optimal. Once the fluctuating range of beacons was determined as marked by red in Fig. 4f, the SERS nanoprobe signals (blue) could be filtered correspondingly, and the signals marked by a black colour were abandoned. Generally, the filtered signals are mainly gathered in a narrower range as marked by two green lines.

To validate the feasibility of the signal filtering method, the repeatability of signals in a series of independent tests was investigated as shown in Fig. S10,† where IL-6 with a concentration of 100 pg mL^{-1} was used. Random twenty measurements were performed by single-point acquisition in each test, and the average intensities of original SERS nanoprobe signals exhibited large fluctuation with an RSD value of 16.3% for twenty independent tests. However, when the collected signals were processed by the signal filtering method, the RSD value of filtered signals was reduced to about 3.5%. The great decrease in RSD values directly revealed the advantage of the signal filtering method in collecting reliable signals, which proved that Raman reporters embedded in magnetic hybrid nanostirrers are very useful for reliable detection. Furthermore, when the signal filtering method is adopted, reliable SERS nanoprobe signals can be quickly obtained using simple single-point measurement, which takes much less time than SERS mapping obviously.

In order to obtain a working curve, the concentration of IL-6 ranging from 10 fg mL^{-1} up to 10 μg mL^{-1} was further characterized by the above method, and the corresponding signals were processed by the signal filtering method. The average Raman spectra of different concentrations of IL-6 are illustrated in Fig. 5a. The beacon signals at 1075 cm^{-1} (MBA) have a small fluctuation, while SERS nanoprobe signals at 1370 cm^{-1} changed with the concentration of IL-6. The average peak intensities at 1370 cm^{-1} were plotted against the concentration of IL-6 as shown in Fig. 5b. The linear dynamic detection range was obtained from 1 pg mL^{-1} to 0.1 μg mL^{-1} (R^2 = 0.989) as shown in the inset of Fig. 5b. Besides, the limit of detection (LOD) could be roughly calculated to be 0.8 pg mL^{-1}, which could be ascribed to the highly brilliant SERS nanoprobes.

Considering that interleukin 6 (IL-6), procalcitonin (PCT) and C-reactive protein (CRP) are often used as a combination of inflammatory factors to evaluate the monitoring indicators of the sepsis cytokine storm period,[47,48] negative control experiments with PCT and CRP, and bovine serum albumin (BSA) were investigated as displayed in Fig. 5c. The Raman spectra show high specificity for IL-6 detection (100 pg mL^{-1}), with only weak SERS signals from the negative controls including PCT (10 ng mL^{-1}), CRP (10 ng mL^{-1}) and BSA (0.5 mg mL^{-1}), which could be attributed to the negligible cross reactivity of the antibodies together with non-specific binding between proteins and SERS nanoprobes.

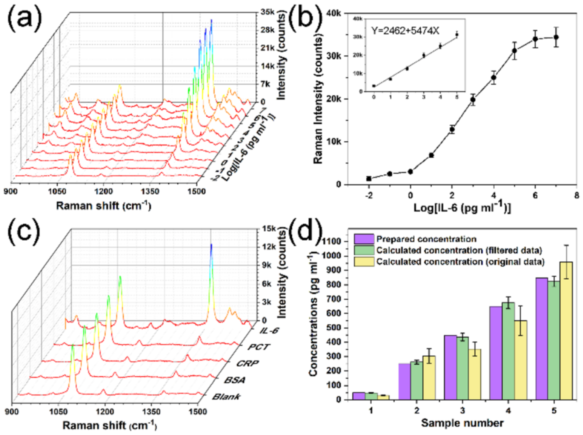

Fig. 5 (a) Average Raman spectra of different concentrations of IL-6 from 10 fg mL^{-1} up to 10 μg mL^{-1}. (b) Reference plot of the Raman intensity at 1370 cm^{-1} *vs.* the logarithm of IL-6 concentrations with the error bar calculated from filtered signals (The inset was the linear part of the reference plot.). (c) SERS spectra of IL-6 (100 pg mL^{-1}), PCT (10 ng mL^{-1}), 10 ng mL^{-1} CRP (10 ng mL^{-1}) and BSA (0.5 mg mL^{-1}). (d) Five prepared concentrations of IL-6 in human serum and their corresponding calculated values. (All error bars were calculated from ten repeats.).

The detection accuracy of the designed microfluidic SERS biosensor was further investigated based on the established working curve in the inset of Fig. 5b. For example, the IL-6 in human serum samples with five concentrations were prepared in advance, and then were detected using the designed microfluidic SERS sensor. Based on the above signal filtering method, the calculated concentrations could be obtained according to the working curve, and data comparison is shown in Fig. 5d. Experimental results present a high degree of accuracy with errors ranging from 4.3% to 7.8% using filtered data. Their overall accuracies were always found to be >92.2%. By contrast, the average values calculated from the original data deviated markedly from the actual values of all tests ranging from 12.9% to 37.6%. The accuracy comparison in the above control bioassay directly indicated that introducing the Raman reporter in the carrier could improve the reliability of the microfluidic SERS sensor greatly.

Conclusions

In summary, when magnetic/plasmonic hybrid nanostirrers embedded with Raman reporters were used as capture carriers, reliable SERS sensing could be achieved by the microfluidic SERS biosensor using IL-6 as model target analytes. After magnetic hybrid nanostirrers were aggregated in a chamber, their SERS signals could act as microenvironment beacons of SERS nanoprobe signals. A signal filtering method was developed based on the relationship between the intensity range of beacons and the signal reproducibility of SERS nanoprobes, in which similar microenvironments could be picked out for reliable SERS nanoprobe signals according to the beacon intensity. Experimental results indicate that the filtered SERS nanoprobe signals exhibited better reproducibility and repeatability than the original SERS nanoprobe signals, which lays a solid foundation for reliable quantitative bioassays. Control experiments indicated that the concentration of IL-6 in serum could be determined accurately according to the established working curve. Our study provides a simple solution for a reliable magnetic-based microfluidic SERS sensor. We believe that the proposed strategy provides good inspiration for the design of reliable particle-based SERS sensors.

Conflicts of interest

There are no conflicts of interest to declare.

Acknowledgements

This work was supported by the National Natural Science Foundation of China (51802080, 51372070), the Natural Science Foundation of Henan Province (162300410022), and the Program for Science & Technology Innovation Talents in University of Henan Province (16HASTIT009).

References

1 D. Mark, S. Haeberle, G. Roth, F. von Stetten and R. Zengerle, *Chem. Soc. Rev.*, 2010, **39**, 1153.

2 E. Livak-Dahl, I. Sinn and M. Burns, *Annu. Rev. Chem. Biomol. Eng.*, 2011, **2**, 325–353.

3 Y. Belotti and C. T. Lim, *Anal. Chem.*, 2021, **93**, 4727–4738.

4 W. Chen, F. Shao and Y. Xianyu, *Small*, 2019, **16**, 1903388.

5 X. Fu, L. Chen and J. Choo, *Anal. Chem.*, 2016, **89**, 124–137.

6 T. Xu, Y. Luo, C. Liu, X. Zhang and S. Wang, *Anal. Chem.*, 2020, **92**, 7816–7821.

7 Z. Liao, Y. Zhang, Y. Li, Y. Miao, S. Gao, F. Lin, Y. Deng and L. Geng, *Biosens. Bioelectron.*, 2019, **126**, 697–706.

8 J. V. Jokerst, A. Raamanathan, N. Christodoulides, P. N. Floriano, A. A. Pollard, G. W. Simmons, J. Wong, C. Gage, W. B. Furmaga, S. W. Redding and J. T. McDevitt, *Biosens. Bioelectron.*, 2009, **24**, 3622–3629.

9 A. Kumar, S. Kim and J. Nam, *J. Am. Chem. Soc.*, 2016, **138**, 14509–14525.

10 W. Zhou, X. Gao, D. Liu and X. Chen, *Chem. Rev.*, 2015, **115**, 10575–10636.

11 J. Li, A. Wuethrich, A. A. I. Sina, H. Cheng, Y. Wang, A. Behren, P. N. Mainwaring and M. Trau, *Nat. Commun.*, 2021, **12**, 1087.

12 K. B. Shanmugasundaram, J. Li, A. I. Sina, A. Wuethrich and M. Trau, *Mater. Adv.*, 2022, **3**, 1459–1471.

13 M. R. Willner, K. S. McMillan, D. Graham, P. J. Vikesland and M. Zagnoni, *Anal. Chem.*, 2018, **90**, 12004–12010.

14 C. Lee and F. Tseng, *Biomicrofluidics*, 2018, **12**, 11502.

15 C. Zong, M. Xu, L. Xu, T. Wei, X. Ma, X. Zheng, R. Hu and B. Ren, *Chem. Rev.*, 2018, **118**, 4946–4980.

16 S. F. Berlanda, M. Breitfeld, C. L. Dietsche and P. S. Dittrich, *Anal. Chem.*, 2021, **93**, 311–331.

17 R. Gao, Z. Cheng, X. Wang, L. Yu, Z. Guo, G. Zhao and J. Choo, *Biosens. Bioelectron.*, 2018, **119**, 126–133.

18 T. Tian, J. Li, Y. Song, L. Zhou and Z. Zhu, *Lab Chip*, 2016, **16**, 1139–1151.

19 M. A. M. Gijs, F. Lacharme and U. Lehmann, *Chem. Rev.*, 2010, **110**, 1518–1563.

20 N. Rezvani Jalal, P. Mehrbod, S. Shojaei, H. I. Labouta, P. Mokarram, A. Afkhami, T. Madrakian, M. J. Los, D. Schaafsma, M. Giersig, M. Ahmadi and S. Ghavami, *ACS Appl. Nano Mater.*, 2021, **4**, 4307–4328.

21 P. H. Lu, Y. D. Ma, C. Y. Fu and G. B. Lee, *Lab Chip*, 2020, **20**, 789–797.

22 S. Bathini, S. Pakkiriswami, R. J. Ouellette, A. Ghosh and M. Packirisamy, *Biosens. Bioelectron.*, 2021, **194**, 113585.

23 X. Bai, L. Wang, J. Ren, X. Bai, L. Zeng, A. Shen and J. Hu, *Anal. Chem.*, 2019, **91**, 2955–2963.

24 A. van Reenen, A. M. de Jong, J. M. den Toonder and M. W. Prins, *Lab Chip*, 2014, **14**, 1966–1986.

25 L. W. Yap, H. Chen, Y. Gao, K. Petkovic, Y. Liang, K. J. Si, H. Wang, Z. Tang, Y. Zhu and W. Cheng, *Nanoscale*, 2017, **9**, 7822–7829.

26 Q. Xiong, C. Y. Lim, J. Ren, J. Zhou, K. Pu, M. B. Chan-Park, H. Mao, Y. C. Lam and H. Duan, *Nat. Commun.*, 2018, **9**, 1743–1754.

27 Q. Xiong, A. E. Lim, Y. Lim, Y. C. Lam and H. Duan, *Adv. Healthcare Mater.*, 2019, **8**, 1801022.

28 W. H. Chong, L. K. Chin, R. L. S. Tan, H. Wang, A. Q. Liu and H. Chen, *Angew. Chem., Int. Ed.*, 2013, **52**, 8570–8573.

29 S. Yang, C. Cao, Y. Sun, P. Huang, F. Wei and W. Song, *Angew. Chem., Int. Ed.*, 2015, **54**, 2661–2664.

30 L. Wan, H. Song, X. Chen, Y. Zhang, Q. Yue, P. Pan, J. Su, A. A. Elzatahry and Y. Deng, *Adv. Mater.*, 2018, **30**, 1707515.

31 Z. Wang, S. Ye, N. Zhang, X. Liu and M. Wang, *Anal. Chem.*, 2019, **91**, 5043–5050.

32 Y. Wang, X. Liu, C. Chen, Y. Chen, Y. Li, H. Ye, B. Wang, H. Chen, J. Guo and X. Ma, *ACS Nano*, 2022, **16**, 180–191.

33 I. Giouroudi and G. Kokkinis, *Nanomaterials*, 2017, **7**, 171.

34 K. Zhang, Y. Wang, M. Wu, Y. Liu, D. Shi and B. Liu, *Chem. Sci.*, 2018, **9**, 8089–8093.

35 A. C. Crawford, A. Skuratovsky and M. D. Porter, *Anal. Chem.*, 2016, **88**, 6515–6522.

36 R. Goodacre, D. Graham and K. Faulds, *Trends Anal. Chem.*, 2018, **102**, 359–368.

37 S. E. J. Bell, G. Charron, E. Cortés, J. Kneipp, M. L. Chapelle, J. Langer, M. Procházka, V. Tran and S. Schlücker, *Angew. Chem., Int. Ed.*, 2020, **59**, 5454–5462.

38 W. Shen, X. Lin, C. Jiang, C. Li, H. Lin, J. Huang, S. Wang, G. Liu, X. Yan, Q. Zhong and B. Ren, *Angew. Chem., Int. Ed.*, 2015, **54**, 7308–7312.

39 A. I. Pérez-Jiménez, D. Lyu, Z. Lu, G. Liu and B. Ren, *Chem. Sci.*, 2020, **11**, 4563–4577.

40 X. Lu, W. Ren, C. Hu, C. Liu and Z. Li, *Anal. Chem.*, 2020, **92**, 12387–12393.

41 Y. Yu, Y. Li, Y. Wang and B. Zou, *Langmuir*, 2018, **34**, 9359–9365.

42 M. Wang, L. He and Y. Yin, *Mater. Today*, 2013, **16**, 110–116.

43 Y. Hu, L. He and Y. Yin, *Angew. Chem., Int. Ed.*, 2011, **50**, 3747–3750.

44 X. Wang, L. Ma, C. Hu, T. Liu, S. Sun, X. Liu and M. Guan, *Nanotechnology*, 2021, **32**, 255702.

45 M. Muhammad, C. Shao and Q. Huang, *Sens. Actuators, B*, 2021, **334**, 129607.

46 Q. Fan, K. Liu, J. Feng, F. Wang, Z. Liu, M. Liu, Y. Yin and C. Gao, *Adv. Funct. Mater.*, 2018, **28**, 1803199.

47 L. Gao, X. Liu, D. Zhang, F. Xu, Q. Chen, Y. Hong, G. Feng, Q. Shi, B. Yang and L. Xu, *Exp. Ther. Med.*, 2017, **13**, 3479–3483.

48 Q. Huang, X. Chen, M. Fan, S. Ruan, S. Peng, R. You, J. Chen and Y. Lu, *Sens. Actuators, B*, 2023, **374**, 132828.